The *ire-1* ER stress-response pathway is required for normal secretory-protein metabolism in *C. elegans*

Modi Safra[1], Shani Ben-Hamo[1], Cynthia Kenyon[2] and Sivan Henis-Korenblit[1,2,*]

[1]The Mina and Everard Goodman Faculty of Life Sciences, Life Sciences Building 212, Room 408, Bar-Ilan University, Ramat Gan, Israel
[2]Department of Biochemistry and Biophysics, Mission Bay Genentech Hall, 600 16th St, Room S312D, University of California, San Francisco, San Francisco, CA 94158-2517, USA

*Author for correspondence (sivankorenblit@gmail.com)

Accepted 11 June 2013
Journal of Cell Science 126, 4136–4146

doi: 10.1242/jcs.123000

Summary

The unfolded protein response (UPR) allows cells to cope with endoplasmic reticulum (ER) stress by adjusting the capacity of the ER to the load of ER-associated tasks. The UPR is important for maintaining ER homeostasis under extreme ER stress. UPR genes are important under normal growth conditions as well, but what they are required for under these conditions is less clear. Using *C. elegans*, we show that the *ire-1/xbp-1* arm of the UPR plays a crucial role in maintaining ER plasticity and function also in the absence of external ER stress. We find that during unstressed growth conditions, loss of *ire-1* or *xbp-1* compromises basic ER functions required for the metabolism of secreted proteins, including translation, folding and secretion. Notably, by compromising ER-associated degradation (ERAD) and phagocytosis, loss of *ire-1* hinders the clearance of misfolded proteins from the ER as well as the clearance of proteins that were secreted into the pseudocoleom. Whereas the basal activity of the UPR is beneficial under normal conditions, it accelerates the pathology caused by toxic Aβ protein in a *C. elegans* model of Alzheimer's disease. Taken together, our findings indicate that UPR genes are critical for maintaining secretory protein metabolism under normal growth conditions.

Key words: UPR, *Caenorhabditis elegans*, ER stress, ERAD, Coelomocytes, Alzheimer's disease

Introduction

The endoplasmic reticulum (ER) fulfills many roles in the cell, including the processing and trafficking of secreted proteins, lipid biosynthesis and metabolism, the production and storage of glycogen and other macromolecules and calcium sequestration. Accordingly, ER homeostasis is essential for proper cellular function; its disruption contributes to many diseases and impairs the development and function of dedicated secretory cells such as plasma cells, insulin secreting cells and liver cells (Lin et al., 2008; Yoshida, 2007).

The ER has a limited capacity and adjusts itself according to the load of its tasks. The accumulation of misfolded proteins in the ER lumen triggers the unfolded protein response (UPR), which initiates processes necessary for restoration of ER homeostasis. This is achieved by expanding the ER itself (Schuck et al., 2009) and by curtailing processes, such as translation, that further burden the ER, thus adjusting the capacity of the ER to the load of ER-associated tasks (Harding et al., 1999).

In *Caenorhabditis elegans*, as in humans, three proteins sense ER stress and activate the UPR: the ribonuclease inositol-requiring protein-1 (IRE-1), the PERK kinase homolog PEK-1 and activating transcription factor-6 (ATF-6). *ire-1* is the only ER-stress sensor gene known in yeast. Upon ER stress, IRE-1 removes an intron from *xbp-1* (X-box binding protein-1) mRNA through unconventional splicing. Spliced *xbp-1* encodes a transcription factor that activates expression of UPR genes, such as chaperones and ER-associated degradation proteins (ERADs) (Calfon et al., 2002; Shen et al., 2001; Urano et al., 2002), which expand the folding capacity of the ER and increase degradation of misfolded proteins. Additional, *xbp-1* independent functions of *ire-1* also exist. These include activation of the cell death machinery (Urano et al., 2000; Yoneda et al., 2001), degradation of ER-localized mRNAs that encode secreted and membrane proteins through the RIDD (regulated Ire1-dependent decay) pathway (Hollien and Weissman, 2006) and induction of autophagosomes (Ogata et al., 2006).

The second branch of the UPR, mediated by PEK-1, a serine/threonine kinase, leads to the phosphorylation of the alpha subunit of the translation initiation factor eIF2. This phosphorylation inhibits the assembly of the 80S ribosome and thereby prevents protein translation initiation, thus reducing the load of proteins to be processed in the ER. In mammals, inhibition of eIF2α selectively increases the translation of ATF4, a transcription factor that regulates stress responses (Scheuner et al., 2001; Shen et al., 2005). ATF6, which mediates the third branch of the UPR, is a basic leucine-zipper transcription factor that is usually retained at the ER membrane. In response to ER stress, mammalian ATF6 transits to the Golgi complex, where it is processed by local proteases to yield an active transcription factor (Ye et al., 2000). At least in mammals, activation of ATF6 induces the expression of genes that increase the folding capacity of the ER.

A functional UPR is known to be required under conditions that abruptly disrupt the balance between ER demand and ER capacity. Most of these studies have been conducted in the presence of chemicals that disrupt protein folding, such as tunicamycin, thapsigargin and dithiothreitol (DTT), or upon

expression of mutant proteins prone to misfolding, all of which abruptly disrupt ER homeostasis. Some evidence for a role of the UPR under physiological conditions has been inferred from studies of model animals lacking central UPR genes (Mori, 2009). However the role fulfilled by the UPR under these conditions has not been established yet.

In this study, we used *C. elegans* to investigate the consequences of UPR deficiency under physiological conditions, in the absence of any additional stress. The *C. elegans* genome encodes conserved homologues of all three known proximal stress-sensing components of the metazoan UPR, each represented by a single homologue, and mutant strains carrying null mutations in these genes are available and viable. By genetically manipulating each branch of the UPR and studying how these manipulations affect ER homeostasis and the life cycle of secreted proteins, we have uncovered a key role for the *ire-1/xbp-1* arm of the UPR in maintaining secretory protein metabolism under basal physiological conditions.

Results

Activation of UPR pathways in ER stress-response mutants

To assess the need for a functional UPR under physiological conditions, we studied animals carrying loss-of-function mutations in central ER stress response genes in each of the UPR arms. We hypothesized that if basal ER homeostasis does not rely on the UPR, inactivation of one of the UPR arms would not disrupt ER homeostasis and hence would not activate the remaining arms of the UPR. In contrast, if a UPR arm is important for the maintenance of ER homeostasis under basal conditions, its inactivation would consequently activate the remaining intact arms of the UPR, in an attempt to restore ER homeostasis.

We assayed the activity of IRE-1 and PEK-1 in various UPR mutants. To assess the activity of IRE-1, we measured the ratio of spliced versus unspliced *xbp-1* transcripts. [*xbp-1* transcript is a direct substrate of the IRE-1 ribonuclease (Calfon et al., 2002; Shen et al., 2001).] This allowed us to compare the ribonuclease activity of IRE-1 in wild-type animals, to its activity in null mutants, in which the *atf-6, pek-1* and *ire-1/xbp-1* UPR genes are disrupted. To determine the activity of PEK-1, we measured the level of phosphorylated eIF2α. [eIF2α is a direct substrate of the PEK-1 kinase.] This allowed us to compare the kinase activity of PEK-1 in wild-type animals to its activity in mutants in which the ATF-6 and IRE-1/XBP-1 arms of the UPR are disrupted.

To analyze the importance of the IRE-1/XBP-1 branch of the UPR, we determined *xbp-1* splicing in *xbp-1(zc12)* mutants, in which this branch has been silenced. The *xbp-1(zc12)* mutant contains a nonsense mutation at codon 34, terminating it before its functional domains, but leaving the *xbp-1* splicing site intact (Richardson et al., 2011). Consistent with previous reports (Richardson et al., 2011), we found that the level of *xbp-1* splicing in *xbp-1(zc12)* mutants was significantly higher than in wild-type animals (Fig. 1A). The level of *xbp-1* splicing observed in *xbp-1(zc12)* mutants was significantly higher than in *atf-6(ok551)* or *pek-1(ok275)* null mutants as well. We did not detect a significant increase in *xbp-1* splicing in *pek-1* mutants compared with wild-type animals. A slightly increased level of *xbp-1* splicing was observed in *atf-6* mutants compared with wild-type animals (Fig. 1A). These results are consistent with previous reports that the levels of *hsp-4* transcripts (*hsp-4* encodes one of the major transcription targets of XBP-1 protein), as measured by qRT-PCR or using a transcriptional reporter, are altered similarly in *atf-6*- and *pek-1*-deficient animals (Shen et al., 2001).

Using the eIF2α phosphorylation assay, we found an increased level of phosphorylated eIF2α in *xbp-1* and in *ire-1(ok799)* null animals relative to wild-type and *atf-6* null animals (Fig. 1B; supplementary material Fig. S1). The phosphorylation of eIF2α in *ire-1* mutants was very sensitive to *pek-1* inactivation (supplementary material Fig. S1). In contrast, the phosphorylation of eIF2α in wild-type animals was most sensitive to RNAi inactivation of *gcn-2*, a cellular eIF2α-kinase that is activated in response to nutrient starvation rather than ER stress (supplementary material Fig. S1).

Taken together, we conclude that the contribution of each UPR arm to ER homeostasis under basal conditions is not equal. Assuming that the level of activation of the UPR arms directly correlates with the need to overcome an imbalance in the ER, then ER homeostasis appears to be most disrupted in *ire-1* mutants and less disrupted in *atf-6* mutants. No significant disruption of ER homeostasis was detected in *pek-1* mutants.

Disruption of ER homeostasis and secretory protein expression in *ire-1* mutants

Increased activation of the remaining arms of the UPR in the absence of one of the ER stress response genes may be sufficient to compensate and restore ER homeostasis and ER function.

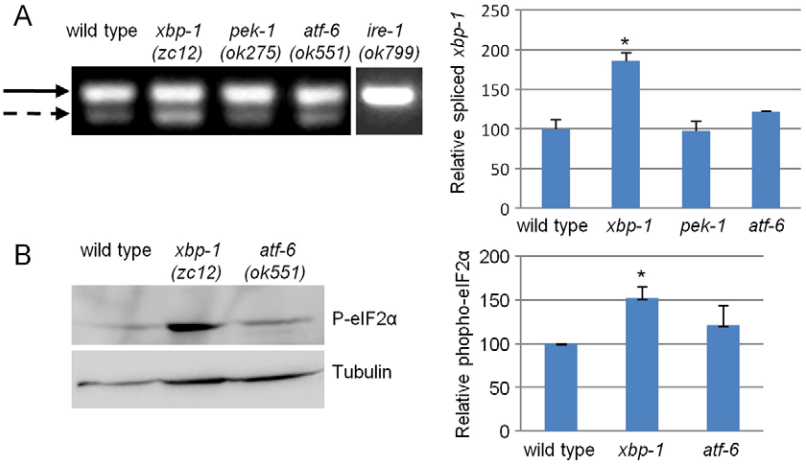

Fig. 1. *xbp-1* deficiency activates the *ire-1* and *pek-1* arms of the UPR. (**A**) Representative steady-state RT-PCR products of unspliced *xbp-1* mRNA (solid arrow) and spliced *xbp-1* mRNA (dashed arrow) of day-1 animals of the indicated genotypes. The *xbp-1* segment was amplified by a single set of PCR primers encompassing the putative intron region. Note that no spliced *xbp-1* mRNA was detected in *ire-1* mutants and that a basal level of spliced *xbp-1* was detected in wild-type animals. The bar graph shows the normalized mean ratio of spliced/unspliced *xbp-1* transcripts in three independent biological experiments. (**B**) Representative western blot of phosphorylated eIF2α and tubulin of day-1 wild-type, *xbp-1* and *atf-6* animals. Bar graph presents the normalized mean ratio of phosphorylated eIF2α levels relative to tubulin in three independent experiments. *$P<0.05$ of the indicated genotype relative to wild type (Student's *t*-test).

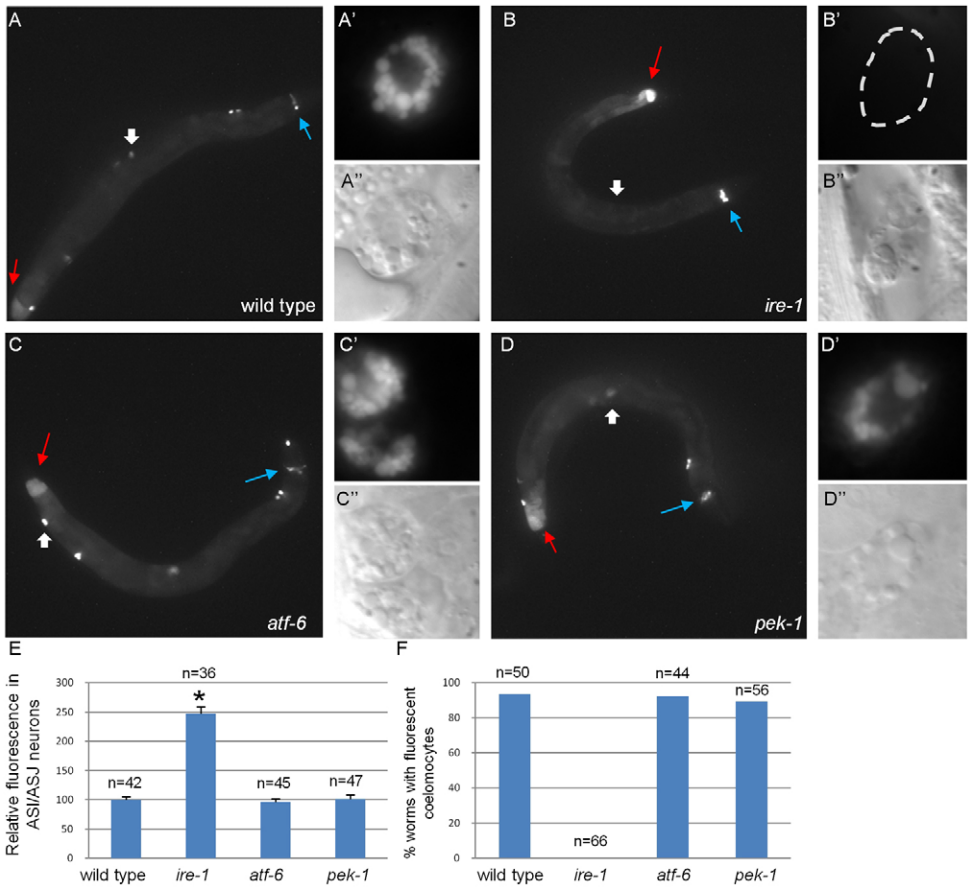

Fig. 2. *ire-1* deficiency alters DAF-28::GFP localization. (**A–D**) Representative fluorescence micrographs (original magnification, 100×) of day-3 wild-type, *ire-1(ok799)*, *atf-6(ok551)* and *pek-1(ok275)* adults harboring an integrated DAF-28::GFP transgene. Blue arrows point to the ASI/ASJ neurons and red arrows indicate the hind gut. Wide white arrows point to coelomocytes, which are shown at high magnification in (A′–D′; fluorescence images) and (A′′–D′′; Nomarski images) (E) Quantification of fluorescence in ASI/ASJ neurons of the different strains, normalized to wild-type fluorescence levels. *$P<0.0001$ (Student's *t*-test). Similar results were obtained in two additional independent experiments. (F) Percentage of worms of the different genetic backgrounds in which fluorescent coelomocytes were detected. *n*, the number of animals analyzed. See supplementary material Fig. S2 for confocal images of DAF-28::GFP within the producing cells of wild-type animals and of *ire-1*, *atf-6* or *pek-1* mutants.

Alternatively, hyperactivation of the remaining arms of the UPR may be indicative of ER dysfunction as a result of chronic ER stress. To differentiate between these two scenarios, we examined the functionality of the ER in mutants defective in each of the three UPR arms. A main function of the ER is to serve as the entry point for proteins into the secretory pathway. Thus, we followed the expression of labeled secreted proteins in transgenic animals upon inactivation of ER stress-response genes. One set of transgenic lines expressed one of the worm insulin-like peptides, DAF-28, fused to GFP from the endogenous *daf-28* promoter. As previously reported (Kao et al., 2007), in wild-type animals DAF-28::GFP was detected in the cells producing it (the ASI and ASJ neurons and the posterior intestine) as well as in the coelomocytes, which are macrophage-like scavenger cells that take up secreted material from the body cavity (Fig. 2A; supplementary material Fig. S2). A second set of transgenic lines expressed GFP fused to a secretion signal (referred to as ssGFP) from the muscle-specific *myo-3* promoter. This strain has been used to follow GFP secretion by muscle cells, and its clearance from the body cavity by the coelomocytes (Fares and Greenwald, 2001). In wild-type animals, ssGFP was detected in the coelomocytes (supplementary material Fig. S3A), but was not clearly detected in the producing cells, probably due to its efficient secretion.

Analysis of both transgenes demonstrated that their overall expression patterns and levels in *pek-1* and *atf-6* mutants were similar to those seen in wild-type animals (Fig. 2; supplementary material Fig. S3). In contrast, mutating *ire-1* appeared to impair protein secretion, as we observed ~2.5-fold higher levels of the DAF-28::GFP reporter in producing ASI and ASJ neurons (Fig. 2E). DAF-28::GFP in the intestinal cells was also higher in *ire-1* mutants compared with wild-type animals, but this was not quantified because of the autofluorescence of this tissue (Fig. 2). Likewise, accumulation of ssGFP in the muscle cells of *ire-1* mutants could not be quantified because some of the muscle-produced ssGFP accumulated in the body cavity of *ire-1(−)* animals, making it difficult to distinguish between fluorescent protein in the body cavity of the animal and fluorescent protein within the adjacent muscle cells (supplementary material Fig. S3). We examined the effects of *ire-1* mutation on a third secreted protein, NLP-21::YFP, a GGARAF neuropeptide expressed ectopically in the ventral cord neurons from the *Punc-129* promoter. As previously reported, in wild-type animals, *Punc-129*::NLP-21::YFP was detected in the ventral cord neurons, and in the coelomocytes (Sieburth et al., 2007). In *ire-1* mutants, the intensity of NLP-21::YFP in the producing cells was threefold higher than in wild-type animals (supplementary material Fig. S3).

We conclude that ER functionality, as judged by the ability to produce and secrete proteins passing through the secretory pathway, is maintained in *pek-1* and *atf-6* mutants, but not in *ire-1* mutants. These data correlate with our findings that ER homeostasis is disrupted in *ire-1* mutants to a greater extent than in *atf-6* and *pek-1* mutants.

IRE-1 is required cell-autonomously for coelomocyte function

Proteins harboring a secretion signal are translated and processed in the ER and secreted into the body cavity of the animal upon

maturation and proper folding. Secreted proteins in the body cavity are eventually taken up and degraded by the coelomocyte cells. In transgenic animals expressing GFP fused to a secreted protein, the GFP is usually detected in the producing cells (before secretion) and in the coelomocytes (upon clearance from the body cavity). By following the expression pattern of DAF-28::GFP and ssGFP, we found that, unlike in wild-type animals, no GFP-labeled coelomocytes were detected in *ire-1* mutants (Fig. 2B,F). Furthermore, in transgenic animals expressing secreted GFP from their muscle cells, GFP accumulated in the body cavity of the animals by day 1 of adulthood (Fig. 3E; supplementary material Fig. S3B).

Why did we fail to observe fluorescent secreted proteins in the coelomocytes? First, we confirmed the presence of coelomocytes in animals lacking *ire-1* both by identifying the cells using Nomarski optics (Fig. 2B′′; supplementary material Fig. S3E) and by labeling them with *Pcup-4*::GFP, which is expressed specifically in the coelomocytes (supplementary material Fig. S4). Next, we explored whether *ire-1* may be a *cup* gene, required in coelomocytes for the uptake of secreted proteins from the body cavity. To this end, we tried to restore *ire-1* expression specifically in the coelomocytes of *ire-1(−)* mutants by expressing *ire-1* using the *hat-1* promoter. This restored detection of the *ire-1/xbp-1* pathway reporter *Phsp-4*::GFP only in coelomocyte cells of tunicamycin-treated *ire-1(−)* transgenic animals (supplementary material Fig. S5). This strongly suggested that the *ire-1*-rescuing construct was expressed in coelomocyte cells, but not in other cells in the animal. Expression of *ire-1* using the *hat-1* promoter in *ire-1(−)* mutants also restored detection of DAF-28::GFP and ssGFP in the coelomocytes (Fig. 3C,F). In addition, it reduced the accumulation of muscle-produced ssGFP in the body cavity of *ire-1(−)* mutants (Fig. 3F). Together, our data suggest that with *ire-1* function intact, the coelomocytes were able to clear GFP from the body cavity of these animals.

IRE-1 is required cell-autonomously for protein secretion

The level of GFP-labeled proteins detected in the coelomocytes is usually used to estimate protein secretion rate. However, since the coelomocytes of *ire-1* mutants are defective, they cannot be used for this purpose. Instead, we estimated protein secretion rate by the amount of labeled protein that accumulated in the body cavity of these animals. To this end, we deliberately prevented coelomocyte protein-uptake function in wild-type animals by introducing *cup* mutations. Notably, we never detected any secreted fluorescence signal taken up from the body cavity of animals by *ire-1(−)* or *cup(−)* coelomocytes. Even upon restoration of *ire-1* expression in the producing cells of otherwise *ire-1(−)* mutants, where high levels of secreted fluorescent protein accumulated in the body cavity, no fluorescent protein was detected in the coelomocyte cells (Fig. 4). These findings suggest that the coelomocyte defect in *ire-1* mutants is severe.

We measured overall fluorescence to compare the amount of labeled protein that accumulated in the body of these animals. Using the *Pmyo-3*::ssGFP transgene, we observed accumulation of muscle-secreted GFP in the body cavity of *ire-1(+);cup-10(−)* and *ire-1(−)* mutants, both of which lack functional

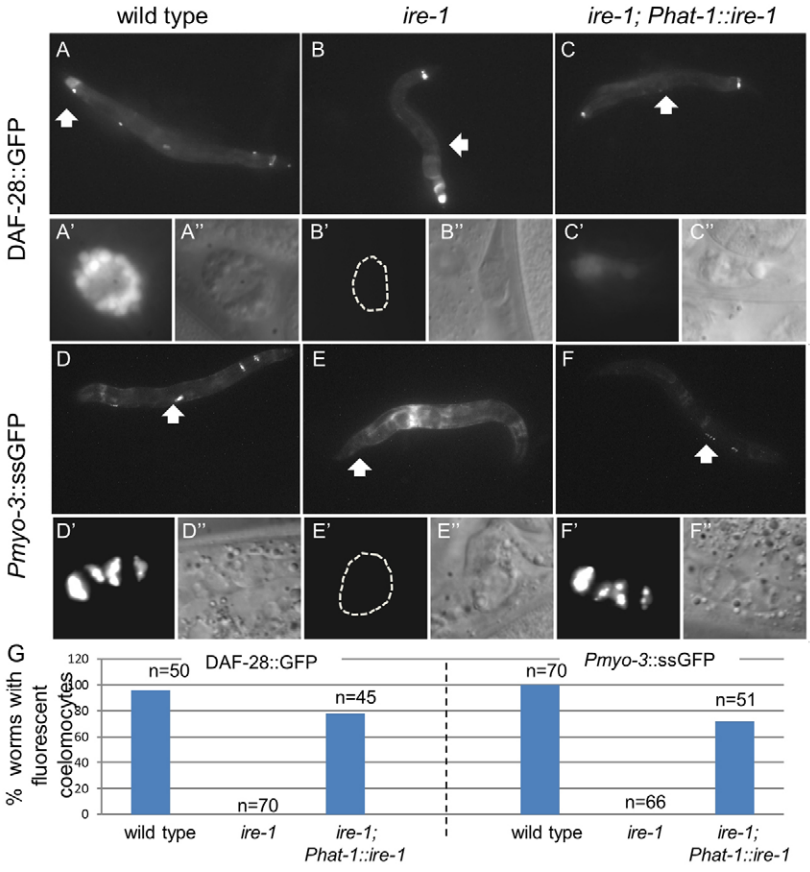

Fig. 3. *ire-1* is required cell-autonomously for coelomocyte function. Representative fluorescence micrographs (original magnification, 100×) of day-3 adults harboring an integrated DAF-28::GFP transgene (A–C) and of day-1 adults harboring an integrated *Pmyo-3*::ssGFP transgene (D–F). In *ire-1(ok799)* mutants no GFP-labeled coelomocytes were detected (B,E). Rescue of *ire-1* in the coelomocytes, achieved by the expression of *Phat-1::ire-1* (see supplementary material Fig. S5 for rescue transgene expression) restored GFP fluorescence in coelomocytes (C,F). Wide white arrows point at coelomocytes shown at higher magnification in A′–F′′ (original magnification, 630×); fluorescence (A′–F′) and Nomarski (A″–F″) photographs are presented. (G) Percentage of animals in which fluorescent coelomocytes were detected in the different genetic backgrounds. *n*, the number of animals analyzed.

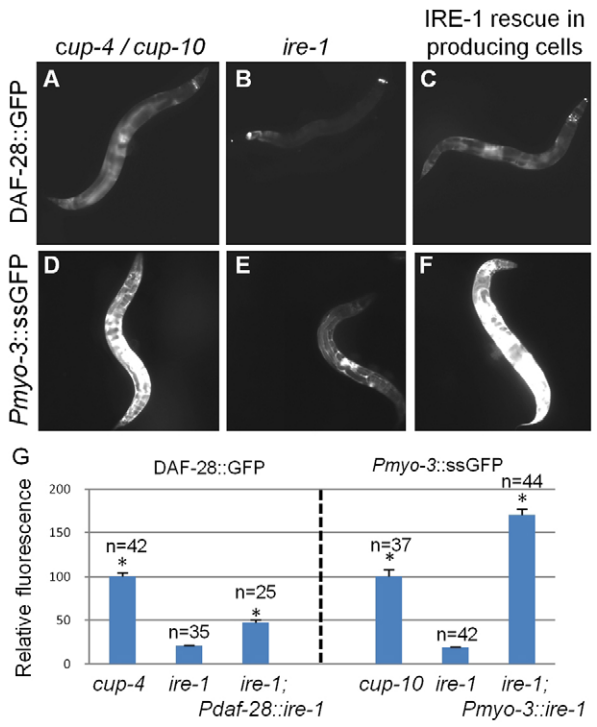

Fig. 4. *ire-1* deficiency reduces accumulation of secreted proteins in the body cavity of coelomocyte-defective animals. Representative fluorescence micrographs (100×) of (A–C) day-3 adults harboring an integrated DAF-28::GFP transgene, and (D–F) day-1 adults harboring a *Pmyo-3*::ssGFP transgene. Coelomocyte-defective *cup-4(ok837)* (A) and *cup-10(ar479)* (D) mutants accumulate secreted proteins in their body cavities. Coelomocyte-defective *ire-1(ok799)* mutants accumulate significantly less GFP in their body cavities (B,E). Expressing *ire-1* specifically in the producing cells of *ire-1(ok799)* mutants using the *daf-28* or the *myo-3* promoters (see supplementary material Fig. S5 for rescue transgene expression) restored accumulation of secreted proteins in the body cavity of *ire-1* mutants (C,F). (G) Bar graph showing the relative mean fluorescence measured in the whole body of the animals of the indicated genotypes. *n*, the number of animals analyzed. Similar results were obtained in two additional independent experiments. **P*<0.0001compared with *ire-1* mutants (Student's *t*-test).

coelomocytes. Significantly higher levels of ssGFP were measured in *ire-1(+); cup-10* mutants than in *ire-1(−)* mutants (Fig. 4D,E,G), suggesting less production of GFP from the muscle cells in *ire-1* mutants. Similarly, using whole-body fluorescence measurements in animals expressing the DAF-28::GFP transgene, we detected relatively low fluorescence levels of DAF-28::GFP in *ire-1(−)* mutants compared with *ire-1(+); cup-4* mutants (Fig. 4A,B,G). Curiously, this was in contrast to the fluorescence levels of DAF-28::GFP in the producing cells that were significantly higher in *ire-1* mutants compared with wild-type animals (Fig. 2E). The accumulation of the secreted proteins in the producing cells, at the expense of their secretion into the body cavity of the animals, suggests that mutations in the *ire-1* pathway interfere with protein secretion.

Next, we followed the expression pattern of DAF-28::GFP within the producing cells, focusing on the ASI/ASJ neurons. In wild-type animals DAF-28::GFP was detected surrounding the periphery of the nucleus as well as in the axons (Fig. 5A; supplementary material Fig. S2). In contrast, in *ire-1* mutants DAF-28::GFP was exclusively detected surrounding the periphery of the nucleus, and was not detected in the axons (Fig. 5A; supplementary material Fig. S2). We suspected that DAF-28::GFP surrounding the periphery of the nucleus represents DAF-28::GFP within the ER. To confirm this, we generated a strain expressing an RFP reporter encompassing an N-terminal secretion signal and an ER retention KDEL signal at the C-terminus in the *daf-28* producing cells (Fig. 5A). Upon co-expression with DAF-28::GFP, we observed that ~85% of DAF-28::GFP colocalized with the ER marker in *ire-1* mutants. In contrast, in wild-type animals, only ~30% of DAF-28::GFP colocalized with the ER marker, as the rest of the DAF-28::GFP was detected outside of the ER (Fig. 5A,B). We conclude that in the absence of *ire-1*, DAF-28::GFP accumulates in the ER of the ASI/ASJ producing cells.

To explore the requirement for *ire-1* in the cells producing the secreted proteins, we restored *ire-1* expression using the *daf-28* promoter or using the *myo-3* promoter. When *ire-1* expression was restored using the *daf-28* promoter, the *ire-1/xbp-1* pathway reporter *Phsp-4*::GFP was again detected in a few head neurons (most likely the ASI/ASJ neurons), in all animals examined. In some animals, *Phsp-4*::GFP expression was also detected in the hind gut (supplementary material Fig. S5C). Expression of *ire-1* using the *myo-3* promoter resulted in the *Phsp-4*::GFP reporter being expressed specifically in the muscle cells of tunicamycin-treated *ire-1(−)* transgenic animals (supplementary material Fig. S5B). These results strongly suggested that the *ire-1*-rescuing construct was specifically expressed in the producing cells, and not in other cells in the animal. In both cases, restoration of IRE-1 in the producing cells significantly increased the accumulation of labeled protein in the body cavity of the animals (Fig. 4C,F,G). Thus, we conclude that *ire-1* functions autonomously to promote secretion by the producing cells.

These findings are consistent with concomitant defects in the cells producing the secreted proteins and in the coelomocytes *of ire-1(−)* mutants. Restoration of *ire-1* in the producing cells restores production and secretion of secreted proteins. However, in the absence of functional coelomocytes, these proteins accumulate in the body cavity of the animal. Expression of *ire-1* specifically in the coelomocytes restores uptake by the coelomocytes. However, with defective producing cells, only a small amount of the proteins intended for secretion reaches the body cavity of the animals, to be cleared by the rescued coelomocytes.

Misfolded secreted proteins accumulate in *ire-1* mutants

Because the normal function of *ire-1* is to decrease the load of misfolded secretory proteins, we sought a way to evaluate the level of misfolded proteins in the animal. One possibility was that misfolding could decrease the *in vivo* fluorescence of a GFP-tagged protein, whose absolute level could be detected by western blotting (Tanudji et al., 2002). If so, then the degree of mismatch between these two methods of protein quantification could reflect the extent of protein misfolding. To explore this, we compared DAF-28::GFP total protein levels and fluorescence levels before and after inactivation of *edem-1*(C47E12.3), an ERAD component, required for the degradation of misfolded proteins in the ER. Treatment with *edem-1* RNAi increased total DAF-28::GFP levels in coelomocyte-defective *cup-4* mutants by more than threefold, as determined by western blotting (Fig. 6A). However, treatment with *edem-1* RNAi did not alter total DAF-28::GFP fluorescence in wild-type animals (Fig. 6B). This

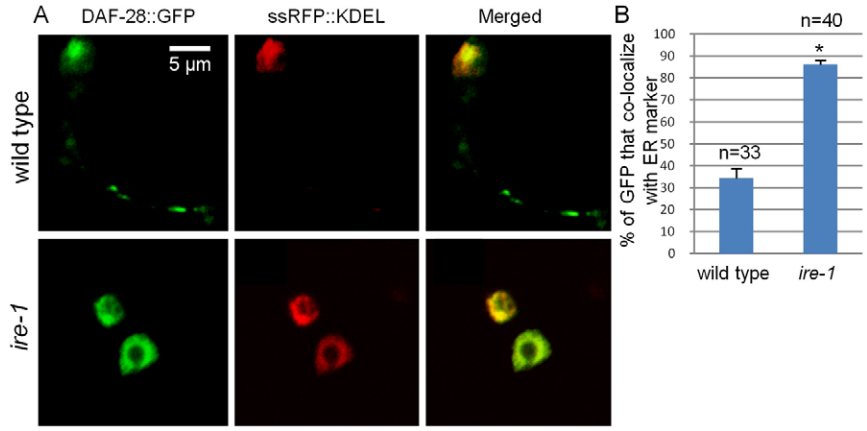

Fig. 5. *ire-1* deficiency traps DAF-28::GFP in the ER. (A) Representative fluorescence confocal micrographs (original magnification, 630×) of a 1.5-µm-thick section of ASI/ASJ neurons in day-3 wild type and *ire-1* mutants co-expressing RFP (fused to a secretion signal and a KDEL-ER retention signal) and DAF-28::GFP. In *ire-1* mutants most of the DAF-28::GFP colocalizes with the ER, whereas in wild-type animals the DAF-28::GFP is detected in the ER as well as in the axons. (B) Colocalization of DAF-28::GFP and the ER marker was quantified. *n*, the number of cells analyzed. **P*<0.0001 (Student's *t*-test).

finding suggests that misfolded, non-fluorescent DAF-28::GFP is normally produced in wild-type animals, but is efficiently removed by the ERAD system. This finding provides a proof of principle that measurements of fluorescence levels versus total protein levels can be used to distinguish between properly folded and misfolded populations of this GFP-tagged protein.

Next, we used this method to compare folded and misfolded populations of DAF-28::GFP in *cup* mutants and *ire-1* mutants, both of which lack functional coelomocytes. We found higher levels of fluorescent DAF-28::GFP in *cup* mutants than in *ire-1* mutants (Fig. 4G). In contrast, using the western blot measurements, we identified significantly higher levels of DAF-28::GFP in *ire-1* mutants than in *cup* single mutants (Fig. 6A). This suggests that a significant portion of DAF-28::GFP protein in *ire-1* mutants is not properly folded, and thus fails to contribute to the overall fluorescence.

Components of the ERAD machinery are well-established downstream targets of the *ire-1/xbp-1* pathway. We hypothesized that the accumulation of misfolded proteins in *ire-1* mutants may result from a compromised ERAD system. Thus, we asked whether *edem-1* inactivation would further increase the level of misfolded DAF-28::GFP in *ire-1* mutants. As predicted, treatment with *edem-1* RNAi did not increase total DAF-28::GFP protein levels in *ire-1* mutants, as determined by western blotting (Fig. 6A), and by fluorescence measurements (Fig. 6B). This suggests that, whereas misfolded DAF-28::GFP is normally produced in wild-type animals and efficiently removed by the ERAD system, in *ire-1* mutants, the ERAD system does not remove misfolded proteins from the ER. These findings are consistent with the interpretation that the *edem-1*-related ERAD machinery is not functioning well in *ire-1* mutants, thus leading to aberrant accumulation of misfolded proteins.

In principle, additional factors, such as increased transcript levels and/or increased translation rates, may contribute to the increased protein levels of DAF-28::GFP in *ire-1* mutants. However, we did not detect significant differences in DAF-28::GFP mRNA levels between *ire-1* and *cup* mutants using quantitative real-time PCR (Fig. 6C). Likewise, it is unlikely that translation rates are increased in *ire-1* mutants, as the level of eIF2α phosphorylation, which limits translation initiation, was increased in *ire-1* mutants (supplementary material Fig. S1). Furthermore, DAF-28::GFP steady-state levels, detected by western blotting, were lower in *ire-1* mutants compared with *cup* mutants upon inactivation of ERAD (Fig. 6A). These conditions reflect DAF-28::GFP synthesis rate, lending further support to the notion that translation rate is slowed down in *ire-1* mutants. We conclude that the increased protein levels of DAF-28::GFP in *ire-1* mutants are mainly due to the increased stabilization of misfolded DAF-28::GFP.

Inactivation of *xbp-1* is sufficient to disrupt ER homeostasis

The major mode of action of *ire-1* upon ER stress is through *xbp-1*, a transcription factor that activates expression of downstream

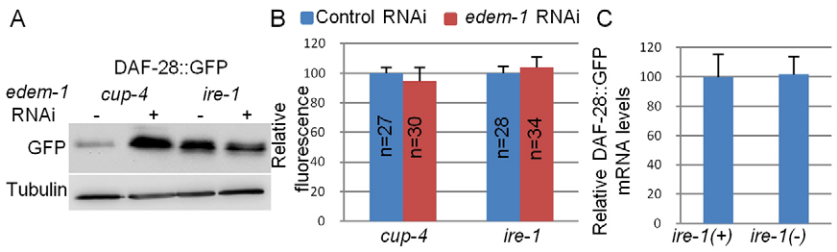

Fig. 6. Misfolded DAF-28::GFP accumulates in *ire-1* mutants. (A) Representative western blot of GFP and tubulin of coelomocyte-defective day-2 *cup-4* and *ire-1(ok799)* mutants harboring an integrated DAF-28::GFP transgene. Animals were treated with control RNAi or *edem-1* RNAi. *edem-1* inactivation increased DAF-28::GFP levels in *cup-4* mutants, but not in *ire-1* mutants, whose basal DAF-28::GFP levels were high even before *edem-1* inactivation. (B) Bar graph showing the relative mean whole-body fluorescence of DAF-28::GFP in day-2 *cup-4* or *ire-1* mutants treated with control RNAi (blue) or *edem-1* RNAi (red). Fluorescence was calculated relative to control RNAi treatment of each strain. *edem-1* inactivation did not increase DAF-28::GFP fluorescence. *n*, the number of animals analyzed. Similar results were obtained in two additional independent experiments. (C) Bar graph showing the average relative mRNA levels of *daf-28::gfp* in *ire-1(+); cup-4(−)* and *ire-1(−)* mutants, measured by qRT-PCR in three independent experiments. *daf-28::gfp* mRNA levels were not increased in *ire-1* mutants ($P>0.45$, Student's *t*-test).

ER-stress-response genes. To assess whether ER homeostasis is disrupted in *xbp-1* mutants, as in *ire-1* mutants, we compared the levels of eIF2α phosphorylation, which reflects the activity of PEK-1. We found that eIF2α phosphorylation was significantly higher in *xbp-1* mutants compared with wild-type animals (Fig. 1B).

Next, we found that the expression of labeled secreted proteins was disrupted in *xbp-1* mutants, as in *ire-1* mutants. As in *ire-1* mutants, no labeled coelomocytes were detected in *xbp-1* mutants expressing muscle-ssGFP or DAF-28::GFP (supplementary material Fig. S6), suggesting that *xbp-1* is also required for coelomocytes to take up secreted proteins. Furthermore, the accumulation of GFP fluorescence in the body cavity of *xbp-1* mutants was significantly lower compared with *cup* mutants. In the case of the DAF-28::GFP strain, an increased fluorescence of DAF-28::GFP in the producing cells was apparent (i.e. the ASI/ASJ neurons and the posterior intestinal cells) (Fig. 7A; supplementary material Fig. S6A). In contrast, total DAF-28::GFP levels in *xbp-1* mutants, as detected by western blotting, were substantially higher compared with *xbp-1(+)* animals (Fig. 7B), indicative of the accumulation of misfolded proteins in these animals. Thus, we conclude that *xbp-1* mutants display similar defects as *ire-1* mutants, resulting in reduced protein secretion, protein folding and coelomocyte function.

ER homeostasis is not equally disrupted in *ire-1* and *xbp-1* mutants, due to autophagy

Even though *ire-1* and *xbp-1* mutants display similar secretion defects, direct comparison of ER homeostasis measures between these two mutants suggested that it was not disrupted equally. Specifically, we found that *ire-1* mutants had higher levels of phosphorylated eIF2α than did *xbp-1* mutants (Fig. 7B). Likewise, *ire-1* mutants accumulated more DAF-28::GFP in the ASI and ASJ neurons than did *xbp-1* mutants (Fig. 7A). These findings suggest that ER homeostasis is disrupted to a greater extent in *ire-1* mutants than in *xbp-1* mutants.

Previous studies in mammalian cell culture demonstrated that IRE1 promotes autophagosome formation in response to tunicamycin-induced ER stress in an *xbp-1*-independent manner (Ogata et al., 2006). We hypothesized that in the absence of *xbp-1*, the imbalanced ER activates IRE-1, which in turn promotes autophagy and possibly ER-phagy, resulting in lysosome/phagosome-mediated degradation of the cargo that accumulated in the stressed ER. This mechanism, which may partially relieve ER stress, is *xbp-1* independent, but cannot be activated in the absence of *ire-1*. To test this hypothesis, we used RNAi to inactivate the Beclin homologue *bec-1*, which is needed for autophagosome formation, and compared DAF-28::GFP levels in the producing cells of wild type, *ire-1* and *xbp-1* mutants. *bec-1* RNAi did not affect DAF-28::GFP fluorescence levels in the ASI/ASJ neurons of wild type or *ire-1* mutants. In contrast, *bec-1* RNAi treatment increased DAF-28::GFP fluorescence levels in the producing cells of *xbp-1* mutants, to levels comparable with those of *ire-1* mutants (Fig. 7A). Thus, it seems that in *xbp-1* mutants, some of the DAF-28::GFP is cleared from the stressed ER through autophagosomes. We propose that autophagosomes formation is initiated by *ire-1* when ER homeostasis is disrupted sufficiently, resulting in the partial clearance of protein that accumulated in the ER. In the absence of *ire-1*, although ER homeostasis is disrupted severely, autophagosome formation cannot be induced, resulting in even higher levels of DAF-28::GFP that cannot be cleared from the ER (see summary model in Fig. 7C).

xbp-1 and *bec-1* depletion delay Aβ-associated toxicity

Our findings suggest that inhibition of the *ire-1/xbp-1* pathway interferes with the translation and secretion of proteins in the secretory pathway even in the absence of exogenous ER stressors. We hypothesized that this activity may be beneficial in diseases associated with the production of toxic secreted proteins, such as Alzheimer's disease. To test this hypothesis, we used a *C. elegans* Alzheimer's disease model in which the

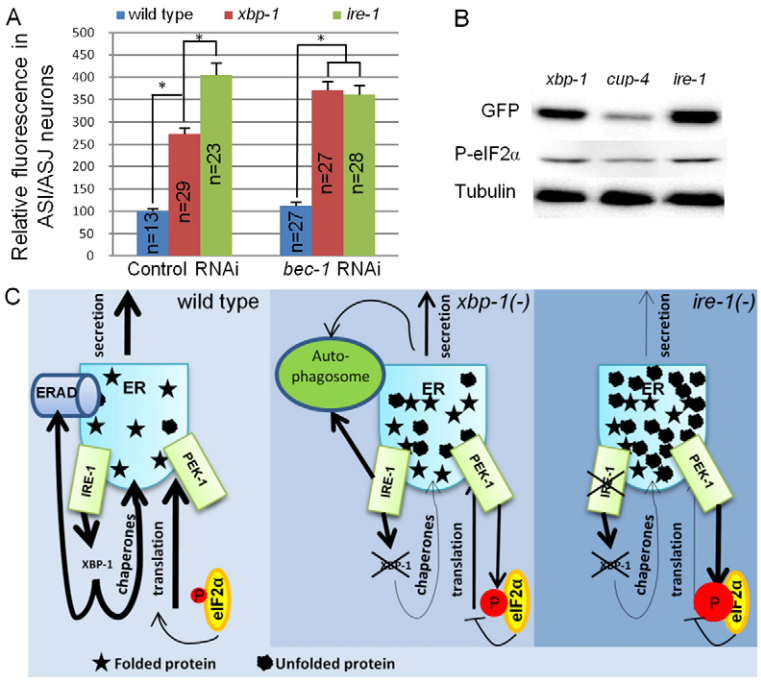

Fig. 7. DAF-28::GFP accumulation in ASI/ASJ neurons is enhanced in *ire-1* mutants and is *bec-1* dependent. (A) Bar graph showing the relative mean fluorescence of DAF-28::GFP measured within the ASI/ASJ DAF-28::GFP-producing cells in wild type, *xbp-1(tm2457)* and *ire-1(ok799)* mutants treated with control or *bec-1* RNAi. *n*, the number of animals analyzed. Similar results were obtained in two additional independent experiments. **P*<0.0001 (Student's *t*-test). (B) Representative western blot of DAF-28::GFP, phosphorylated eIF2α and tubulin of day-1 *xbp-1, cup-4* and *ire-1* mutants expressing the *daf-28::gfp* transgene. (**C**) Model for disruption of ER homeostasis in *ire-1* and *xbp-1* mutants. Normally, *xbp-1* transcribes target genes that promote ER homeostasis by preventing the accumulation of misfolded proteins in the ER. In *xbp-1*-deficient animals, misfolded proteins are not cleared by ERAD. These accumulate and activate IRE-1. *ire-1* cannot activate *xbp-1*. Instead, it induces autophagosomes that clear some of the misfolded proteins from the ER. In *ire-1*-deficient animals, misfolded proteins accumulate in the ER but the ERAD and *ire-1*-induced autophagosomes do not clear them. High levels of misfolded proteins burden the ER, activate the remaining UPR arms and interfere with protein secretion.

expression of the Aβ peptide can be induced in its muscle cells upon temperature shift (Link et al., 2003). This Aβ peptide is equivalent to the 43 amino acid tail cleaved off the terminus of the amyloid precursor protein (APP), which is thought to be toxic to cells. Consistent with this, otherwise wild-type worms expressing this Aβ peptide are paralyzed ~24 hours after Aβ induction (Link et al., 2003). We found that *xbp-1* RNAi treatment delayed paralysis in this inducible Aβ *C. elegans* strain by ~3 hours (Fig. 8A). This delay correlated with reduced Aβ protein levels (Fig. 8B,C), but did not correlate with any change in Aβ mRNA levels (Fig. 8C). Thus, this reduced Aβ toxicity may derive from the inhibition of translation in the *ire-1/xbp-1* mutants.

Based on our finding that RNAi against *bec-1* further enhanced the secretory defects in *xbp-1* mutants, we hypothesized that reduction of autophagosome formation in an *xbp-1*-mutant background would further delay the toxicity of Aβ as well. To test this, Aβ-expressing *xbp-1* mutants were treated with control or *bec-1* RNAi. We found that RNAi against *bec-1* further delayed the paralysis of *xbp-1* mutants by ~2 hours (Fig. 8E). Importantly, *bec-1* RNAi did not delay the paralysis of *ire-1* animals or wild-type animals expressing the Aβ peptide (Fig. 8D,F). Thus, counterintuitively, inhibition of the UPR through *xbp-1* inactivation, in conjunction with inhibition of autophagosome formation, might be beneficial in diseases associated with toxic secreted proteins. We speculate that this is due to enhanced interference with the production of the toxic proteins in the ER.

Discussion

The *ire-1/xbp-1* UPR pathway fulfills crucial functions required for embryonic development and viability in *Drosophila*, *Xenopus* and mice (Reimold et al., 2000; Souid et al., 2007; Zhao et al., 2003). A functional UPR is also required for the development of hepatic, bone marrow and B cells, as well as for yeast cytokinesis (Bicknell et al., 2007; Hu et al., 2009; Lee et al., 2008; Reimold et al., 2001; Todd et al., 2008). In *C. elegans*, *ire-1/xbp-1*-depleted animals are hypersensitive to ER stress (Shen et al., 2001) and pathogens (Richardson et al., 2010) and have a shortened lifespan (Henis-Korenblit et al., 2010). However, these mutants are viable under physiological conditions, generating a unique opportunity to study the cellular requirements of this pathway at the organism level.

One of the main functions of the ER is to serve as an entry point into the secretory pathway of the cell. In this study, we used the model organism *C. elegans* to investigate the physiological requirement of UPR signaling for ER homeostasis and for the life-cycle of proteins passing through the secretory pathway under standard growth conditions and in an Alzheimer's disease model. Using loss-of-function mutations disrupting the *ire-1*, *pek-1* and *atf-6* arms of the UPR, we found that elimination of one UPR arm leads to increased activation of the remaining UPR arms in adult animals. This is consistent with a comprehensive microarray analysis of UPR mutants that demonstrated that some genes associated with ER-stress conditions were upregulated in some UPR mutants (Shen et al., 2005).

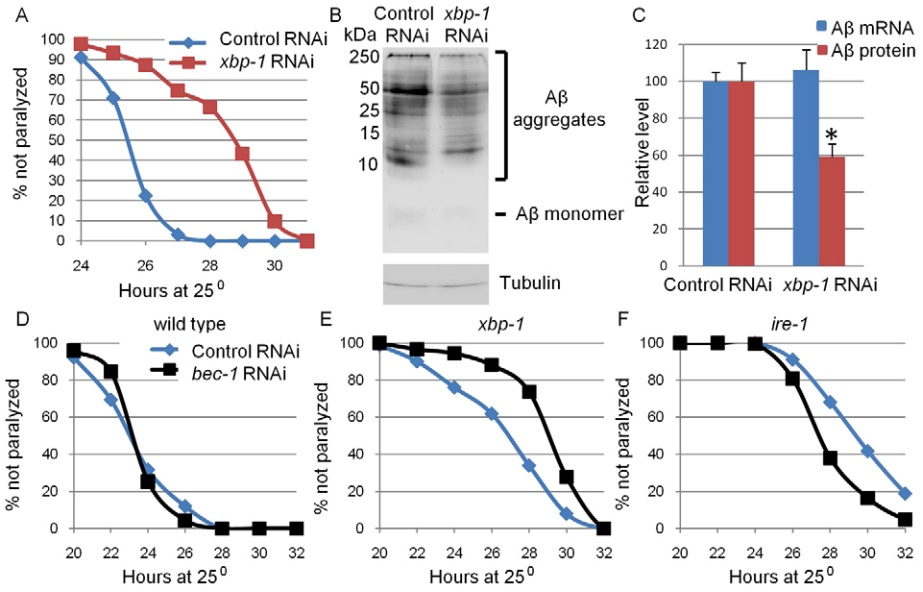

Fig. 8. *xbp-1* inactivation reduces Aβ levels and delays paralysis. Eggs from animals expressing inducible Aβ in their muscles were grown at the permissive temperature and treated with control RNAi, *xbp-1* RNAi or *bec-1* RNAi for 48 hours. Animals were then shifted to the non-permissive temperature and Aβ expression was induced. (A) Paralyzed animals were scored each hour between 24 to 31 hours after temperature shift. *xbp-1* RNAi significantly delayed paralysis of Aβ-expressing animals (control RNAi: mean=25.9 hours; n=124; *xbp-1* RNAi: mean=28.7 hours, n=134; $P<0.0001$) (B) Representative western blots of Aβ (top panel) and tubulin (bottom panel) of Aβ-expressing animals treated with control RNAi and *xbp-1* RNAi. Most of the Aβ protein was detected in high-molecular-mass aggregates. A very weak Aβ band was in a monomeric form. (C) Bar graph showing the average relative protein and mRNA levels of Aβ in control and *xbp-1*-RNAi-treated animals measured by qRT-PCR (blue bars) and western blot (red bars). Measurements were normalized to actin mRNA and tubulin protein levels, respectively. Values are the average of three independent experiments. *$P>0.05$, Student's t-test. (D–F) Paralyzed animals were scored every 2 hours between 20 and 32 hours after temperature shift. (D) *bec-1* RNAi did not delay paralysis of wild-type Aβ-expressing animals (control RNAi: mean=24.1 hours; n=600; *bec-1* RNAi: mean=24.2 hours, n=317; P=0.27). (E) *bec-1* RNAi significantly delayed paralysis of Aβ-expressing *xbp-1* mutants (control RNAi: mean=27.4 hours, n=577; *bec-1* RNAi: mean=29.6 hours, n=488; $P<0.0001$). (F) *bec-1* RNAi did not delay paralysis of Aβ-expressing *ire-1* mutants (control RNAi: mean=30.4 hours, n=380; *bec-1* RNAi: mean=28.8 hours, n=250; $P<0.0001$).

Elimination of the *ire-1*, *pek-1* and *atf-6* arms of the UPR leads to increased activation of the remaining UPR arms in adult animals, albeit to different extents. Consistent with a previous report (Richardson et al., 2011), we found that inactivation of the *ire-1*/*xbp-1* pathway significantly increased the UPR in adult animals. This was reflected in increased splicing of the *xbp-1* transcript by IRE-1 and increased level of phosphorylation of eIF2α by PEK-1. Nevertheless, ER homeostasis and function were not restored in *ire-1* and *xbp-1* mutants, in spite of strong activation of the remaining UPR arms. In our hands, no significant disruption in ER function or activation of the UPR was detected in *pek-1* mutants. In contrast, although *atf-6* mutants maintained ER function, weak activation of the UPR was observed in *atf-6* mutants. We propose that activation of the UPR arms in *atf-6* mutants, whose ER homeostasis was mildly disturbed, served as a compensatory response that successfully restored ER homeostasis and maintained ER function. Our findings indicate that animals are constantly subjected to a basal level of ER stress and that UPR genes, and especially the *ire-1/xbp-1* arm of the UPR, are required to maintain ER homeostasis under these physiological conditions.

In *ire-1* and *xbp-1* mutants, high levels of labeled secreted proteins were detected in the producing cells, suggesting a secretion defect. Previously, the glutamate receptor was shown to require *xbp-1* to exit the ER and take its place in the plasma membrane in *C. elegans* (Shim et al., 2004). However, the same study demonstrated that this phenomenon was not general, as other transmembrane proteins reached their destination in the outer membrane in the absence of *xbp-1*. This unique feature of the glutamate receptor could be attributed to its tendency to fold improperly and its requirement for additional cofactors as it exits the ER (Vandenberghe and Bredt, 2004). However, *xbp-1* appears to be more generally required for protein secretion, as we found that the *ire-1/xbp-1* pathway was required for efficient protein secretion of three independent proteins expressed in the muscle, the intestine and neurons.

Our findings suggest that misfolded proteins accumulate in *ire-1/xbp-1* mutants. We were able to draw this conclusion by comparing DAF-28::GFP levels of wild type and *ire-1*/*xbp-1* mutants expressing the DAF-28::GFP transgene in two different ways: by fluorescence intensity in the animal, which reflects the level of properly folded protein, and by western blotting, which detects DAF-28::GFP irrespective of its folding state. In this way, we found that *ire-1*/*xbp-1* mutants accumulate more DAF-28::GFP than control animals, however, most of this protein is in a misfolded state in which the GFP region cannot contribute to the fluorescence measurements.

Incorrect folding of proteins in the ER is a normal phenomenon. However, typically, misfolded proteins are cleared by the ERAD machinery and thus do not accumulate. Interestingly, inactivation of ERAD did not further increase the level of DAF-28::GFP protein in *ire-1*/*xbp-1* mutants. This may indicate that the majority of DAF-28::GFP in these animals is properly folded and thus not affected by ERAD. However, given the lack of correlation between the fluorescence of DAF-28::GFP and DAF-28::GFP increased protein levels, this is unlikely. Instead, we favor the interpretation that the ERAD machinery in these animals is inactive to begin with. As a result, DAF-28::GFP levels are not further increased in these mutants upon ERAD inactivation. This interpretation is consistent with the fact that genes encoding ERAD components, such as *hrd-1* and *edem-1*, are XBP-1 target genes (Yamamoto et al., 2007). Curiously, microarray studies comparing constitutive and inducible transcriptional changes in *ire-1* and *xbp-1* mutants demonstrated that *ire-1* and *xbp-1* were not required for their constitutive transcription under physiological conditions (Shen et al., 2005). Nevertheless, our findings suggest that even if ERAD components are actively transcribed in *ire-1* and *xbp-1* mutants, the ERAD machinery in these mutants does not function properly, leading to the accumulation of misfolded proteins instead of their degradation.

In addition to the reduced ability of cells to fold and secrete proteins into the pseudocoelom, we find that the ability of *ire-1* and *xbp-1* mutants to clear proteins that have been deposited in the pseudocoelom is also compromised. Using cell-specific rescue of *ire-1* expression, we found that *ire-1* is required cell-autonomously in specialized scavenger cells called coelomocytes to enable their efficient uptake of secreted material from the body cavity. This further supports a previous report that identified a *C. elegans* Derlin homolog, associated with ERAD function, as being required for coelomocyte function (Schaheen et al., 2009). It is not clear why coelomocyte scavenger function would be disrupted in the absence of *ire-1* and *xbp-1*. Given that coelomocytes endocytose a wide variety of secreted proteins in the animal, it is possible that their level of membrane-protein trafficking and recycling is higher than that of many other cell types. Therefore their scavenger function may be particularly sensitive to reduced ER efficiency.

This coelomocyte defect explains our counterintuitive finding that although protein secretion is severely disrupted in *ire-1* and *xbp-1* mutants, some secreted proteins can be detected in high amounts in the body cavity of *ire-1* and *xbp-1* animals compared with control animals (this is the case for ssGFP expressed from the muscle cells). Thus, if proteins leak from the producing cells into the pseudoceolom, even at a very low rate, these proteins will not be cleared from the body cavity because of the coelomocyte defect, and will accumulate there.

In *ire-1* and *xbp-1* mutants, the *pek-1* UPR pathway is activated and protein secretion and coelomocyte function are disrupted. Thus, it could be that these defects of *ire-1* and *xbp-1* mutants are mediated by the compensatory activation of the remaining UPR pathways. However, we were unable to support or disprove this hypothesis. This was because treatment of *ire-1* mutants, expressing the DAF-28::GFP transgene, with *atf-6* or *pek-1* RNAi from the L3 stage did not alter protein secretion or coelomocyte function (data not shown). More robust treatment with *atf-6* and *pek-1* RNAi was incompatible with the animals' development.

Interestingly, *ire-1* mutants accumulate higher levels of DAF-28::GFP in their producing cells than do *xbp-1* mutants, suggesting that the secretory defect of *ire-1* is more severe than that of *xbp-1*. Furthermore, *ire-1* mutants exhibit higher levels of phosphorylated eIF2α than do *xbp-1* mutants, reflecting increased activity of the PEK-1 UPR pathway. These finding suggest that *ire-1* mutants experience more ER stress than do *xbp-1* mutants, and thus that *xbp-1*-independent functions of *ire-1* also contribute to the maintenance of physiological ER homeostasis.

What *xbp-1*-independent functions of *ire-1* might contribute to the maintenance of ER homeostasis? One plausible hypothesis is that autophagosome formation, mediated by *ire-1* independently of *xbp-1*, might counteract and partially relieve the accumulation of secreted proteins in the ER. In support of this hypothesis, we

find that inactivation of the *C. elegans* Beclin homologue, which is needed for phagosome formation, further disrupted ER homeostasis in *xbp-1* mutants. Furthermore, since *bec-1* inactivation increased DAF-28::GFP levels in the producing cells, matching them to those detected in *ire-1* mutants, autophagy may account for most of the difference in ER homeostasis between *ire-1* and *xbp-1* mutants.

In summary, our data support the idea that UPR signaling, and especially *ire-1/xbp-1* signaling, are crucial for ER homeostasis and its ability to metabolize secretory proteins not only under conditions of environmental stress, but also under normal growth conditions. Under these conditions, *ire-1* and *xbp-1* deficiency reduces basic ER functions, including translation, folding, secretion and degradation of proteins passing through the secretory pathway. These findings may explain a wide range of physiological defects associated with UPR deficiencies (Bicknell et al., 2007; Fonseca et al., 2012; Henis-Korenblit et al., 2010; Hu et al., 2009; Lee et al., 2008; Reimold et al., 2000; Reimold et al., 2001; Richardson et al., 2010; Souid et al., 2007; Todd et al., 2008; Zhao et al., 2003).

Finally, although disruption of the UPR impairs many aspects of normal cellular function, it may be beneficial under extreme circumstances, such as disease onset associated with toxic protein production. Specifically, we find that reducing *xbp-1* levels in a *C. elegans* Alzheimer's disease model limited the levels of the toxic peptide Aβ and delayed its toxicity. Inhibition of the UPR through *xbp-1* inactivation in conjunction with inhibition of autophagosome formation further delayed Aβ toxicity. We speculate that this delay is due to enhanced interference with the production and processing of the toxic proteins in the ER. These findings may have implications for higher organisms, because targeting of *xbp-1* in a Huntington's disease model in mice proved to be protective as well (Vidal et al., 2012). Thus, better understanding of the consequences of UPR inactivation in the context of normal growth and disease, in *C. elegans* and in higher organisms, may lead to new therapeutic strategies to combat diseases that are associated with the production of toxic proteins in the ER.

Materials and Methods

Strains

Strains were cultured as described previously (Brenner, 1974) other than strain CL4176, which was maintained at 15℃ and shifted to 25℃ for Aβ induction. A list of strains used in this study is provided in supplementary material Table S1.

xbp-1 splicing

On day 1 of adulthood, animals were collected for RNA extraction, purification and reverse transcription, using random 9-mers and standard protocol. A primers set encompassing the noncanonical intron of the *xbp-1* transcript was used, giving rise to two PCR products of amplified spliced and unspliced *xbp-1* transcript (primers: 5′-TCCGCTTGGGCTCTTGAGATGTTC-3′ and 5′-TGTCGTCGTCGGAGGAGAGGATCG-3′). PCR products were visualized on a 2% agarose gel stained with ethidium bromide. Gels were scanned and analyzed using ImageJ software.

Fluorescence microscopy and quantification

Animals were anaesthetized on 2% agarose pads containing 2 mM levamisol.

Images were taken with a CCD digital camera using a Nikon 90i fluorescence microscope. For each trial, exposure time was calibrated to minimize the number of saturated pixels and was kept constant through the experiment. The NIS element software was used to quantify mean fluorescence intensity as measured by intensity of each pixel in the selected area.

Confocal microscopy

Confocal images were taken using an LSM 510 confocal scanning microscope (Carl Zeiss, Jena, Germany) with a 63 NA objective lens. Worms were mounted on 2% agarose pads containing 2 mM levamisol. Sections of 1.5 µm were taken. Colocalization was measured using ImageJ software.

Quantitative RT-PCR analysis

Animals were raised at 20℃ until day 1 of adulthood, unless indicated otherwise. On day 1 animals were collected for RNA extraction. RNA extraction, purification and reverse transcription were carried out using standard protocols. Real-time PCR was performed using Maxima SYBR (Fermentas) in a StepOnePlus instrument. Transcript levels of *act-1* were used for normalization.

Primers used for qPCR:

act-1: 5′-CCAATCCAAGAGAGGTATCCTTAC-3′ and 5′-CATTGTAGAAGGTGTGATGCCAG-3′; *gfp*: 5′-CTGTTCCATGGCCAACACTTG-3′ and 5′-GTCATGCTGTTTCATATGATCTGG-3′; Aβ: 5′-CCGACATGACTCAGGATATGAAGT-3′ and 5′-CACCATGAGTCCAATGATTGCA-3′.

Plasmids and transgenic animals

The *ire-1* coding sequence was amplified from cDNA and cloned into the *Nhe*I and *Kpn*I sites in the L3691/promoterless plasmid. Genomic DNA-amplified promoters were inserted upstream of the *ire-1* coding sequence (CDS) as follows: *Pdaf-28* (~3.3 kb), *Phat-1* (~2.9 kb), *Pmyo-3* (~2.6 kb).

To generate *Pdaf-28*::RFP::KDEL, the *ire-1* CDS of L3691/*Pdaf-28::ire-1* was replaced with a PCR product of RFP fused to KDEL followed by a stop codon. The *ire-1* CDS was excised such that the first 118 amino acids of *ire-1*, including the signal peptide, was fused in frame to the RFP-KDEL. Germline transformations were performed by injection of 25 ng/µl plasmids and 100 ng/µl of *rol-6(su1006)* as a co-transformation marker.

Western blot

A similar number of animals were boiled in protein sample buffer containing 2% SDS. Proteins were separated using standard PAGE separation, transferred to a nitrocellulose membrane and detected by western blotting using the following antibodies: anti-GFP (Roche, 1:1000), anti-tubulin (DHSB, 1:5000), anti-phospho-eIF2α (Cell signaling, 1:500) and anti-Aβ (6E10, Covans, 1:1000).

Paralysis assay

Synchronized worms of strain CL4176 laid eggs on plates RNAi, which were grown at 15℃. After ~48 hours the worms were shifted to 25℃ for induction of Aβ expression. After 24 hours animals were scored hourly for paralysis or harvested for western blot and RT-PCR analysis.

Statistical analysis

Error bars represent the standard error of the mean (s.e.m.). *P*-values were calculated using the unpaired Student's *t*-test. Statistical analysis of paralyzed worms was done using Statview 5.0.1 software (SAS) and *P*-values were calculated using the log-rank Mantel–Cox method.

Acknowledgements

Some nematode strains used in this work were provided by the Caenorhabditis Genetics Center, which is funded by the NIH National Center for Research Resources (NCRR) and by Dr Shohei Mitani, National Bioresource Project for the nematode, Tokyo Women's Medical University School of Medicine, Japan. We thank Dr Hanna Fares (University of Arizona, Tucson, AZ) for coelomocyte marker strains, Prof. Peter Naredi (Umea University, Sweden) for the DAF-28::GFP-expressing strain and Dr QueeLim Ch'ng (King's College, London, UK) for the NLP-21::YFP.

Author contributions

M.S., C.K. and S.H.K. conceived and designed the experiments. M.S. and S.B.H. performed the experiments. M.S., C.K. and S.H.K. analyzed the data and wrote the manuscript.

Funding

This study was supported by the National Institutes of Health [grant number R37 AG011816 to C.K.]; the United States–Israel Binational Science Foundation [grant number 2009356 to S.H.K. and C.K.]; the Israel Science Foundation [grant number 1749/11 to S.H.K.]; and a Marie Curie International Reintegration Grant [grant number 256551 to S.H.K.]. Deposited in PMC for release after 12 months.

Supplementary material available online at
http://jcs.biologists.org/lookup/suppl/doi:10.1242/jcs.123000/-/DC1

References

Bicknell, A. A., Babour, A., Federovitch, C. M. and Niwa, M. (2007). A novel role in cytokinesis reveals a housekeeping function for the unfolded protein response. *J. Cell Biol.* **177**, 1017-1027.

Brenner, S. (1974). The genetics of Caenorhabditis elegans. *Genetics* **77**, 71-94.

Calfon, M., Zeng, H., Urano, F., Till, J. H., Hubbard, S. R., Harding, H. P., Clark, S. G. and Ron, D. (2002). IRE1 couples endoplasmic reticulum load to secretory capacity by processing the XBP-1 mRNA. *Nature* **415**, 92-96.

Fares, H. and Greenwald, I. (2001). Genetic analysis of endocytosis in Caenorhabditis elegans: coelomocyte uptake defective mutants. *Genetics* **159**, 133-145.

Fonseca, S. G., Urano, F., Weir, G. C., Gromada, J. and Burcin, M. (2012). Wolfram syndrome 1 and adenylyl cyclase 8 interact at the plasma membrane to regulate insulin production and secretion. *Nat. Cell Biol.* **14**, 1105-1112.

Harding, H. P., Zhang, Y. and Ron, D. (1999). Protein translation and folding are coupled by an endoplasmic-reticulum-resident kinase. *Nature* **397**, 271-274.

Henis-Korenblit, S., Zhang, P., Hansen, M., McCormick, M., Lee, S. J., Cary, M. and Kenyon, C. (2010). Insulin/IGF-1 signaling mutants reprogram ER stress response regulators to promote longevity. *Proc. Natl. Acad. Sci. USA* **107**, 9730-9735.

Hollien, J. and Weissman, J. S. (2006). Decay of endoplasmic reticulum-localized mRNAs during the unfolded protein response. *Science* **313**, 104-107.

Hu, C. C., Dougan, S. K., McGehee, A. M., Love, J. C. and Ploegh, H. L. (2009). XBP-1 regulates signal transduction, transcription factors and bone marrow colonization in B cells. *EMBO J.* **28**, 1624-1636.

Kao, G., Nordenson, C., Still, M., Rönnlund, A., Tuck, S. and Naredi, P. (2007). ASNA-1 positively regulates insulin secretion in C. elegans and mammalian cells. *Cell* **128**, 577-587.

Lee, A. H., Scapa, E. F., Cohen, D. E. and Glimcher, L. H. (2008). Regulation of hepatic lipogenesis by the transcription factor XBP1. *Science* **320**, 1492-1496.

Lin, J. H., Walter, P. and Yen, T. S. (2008). Endoplasmic reticulum stress in disease pathogenesis. *Annu. Rev. Pathol.* **3**, 399-425.

Link, C. D., Taft, A., Kapulkin, V., Duke, K., Kim, S., Fei, Q., Wood, D. E. and Sahagan, B. G. (2003). Gene expression analysis in a transgenic Caenorhabditis elegans Alzheimer's disease model. *Neurobiol. Aging* **24**, 397-413.

Mori, K. (2009). Signalling pathways in the unfolded protein response: development from yeast to mammals. *J. Biochem.* **146**, 743-750.

Ogata, M., Hino, S. i., Saito, A., Morikawa, K., Kondo, S., Kanemoto, S., Murakami, T., Taniguchi, M., Tanii, I., Yoshinaga, K. et al. (2006). Autophagy is activated for cell survival after endoplasmic reticulum stress. *Mol. Cell. Biol.* **26**, 9220-9231.

Reimold, A. M., Etkin, A., Clauss, I., Perkins, A., Friend, D. S., Zhang, J., Horton, H. F., Scott, A., Orkin, S. H., Byrne, M. C. et al. (2000). An essential role in liver development for transcription factor XBP-1. *Genes Dev.* **14**, 152-157.

Reimold, A. M., Iwakoshi, N. N., Manis, J., Vallabhajosyula, P., Szomolanyi-Tsuda, E., Gravallese, E. M., Friend, D., Grusby, M. J., Alt, F. and Glimcher, L. H. (2001). Plasma cell differentiation requires the transcription factor XBP-1. *Nature* **412**, 300-307.

Richardson, C. E., Kooistra, T. and Kim, D. H. (2010). An essential role for XBP-1 in host protection against immune activation in C. elegans. *Nature* **463**, 1092-1095.

Richardson, C. E., Kinkel, S. and Kim, D. H. (2011). Physiological IRE-1-XBP-1 and PEK-1 signaling in Caenorhabditis elegans larval development and immunity. *PLoS Genet.* **7**, e1002391.

Schaheen, B., Dang, H. and Fares, H. (2009). Derlin-dependent accumulation of integral membrane proteins at cell surfaces. *J. Cell Sci.* **122**, 2228-2239.

Scheuner, D., Song, B., McEwen, E., Liu, C., Laybutt, R., Gillespie, P., Saunders, T., Bonner-Weir, S. and Kaufman, R. J. (2001). Translational control is required for the unfolded protein response and in vivo glucose homeostasis. *Mol. Cell* **7**, 1165-1176.

Schuck, S., Prinz, W. A., Thorn, K. S., Voss, C. and Walter, P. (2009). Membrane expansion alleviates endoplasmic reticulum stress independently of the unfolded protein response. *J. Cell Biol.* **187**, 525-536.

Shen, X., Ellis, R. E., Lee, K., Liu, C. Y., Yang, K., Solomon, A., Yoshida, H., Morimoto, R., Kurnit, D. M., Mori, K. et al. (2001). Complementary signaling pathways regulate the unfolded protein response and are required for C. elegans development. *Cell* **107**, 893-903.

Shen, X., Ellis, R. E., Sakaki, K. and Kaufman, R. J. (2005). Genetic interactions due to constitutive and inducible gene regulation mediated by the unfolded protein response in C. elegans. *PLoS Genet.* **1**, e37.

Shim, J., Umemura, T., Nothstein, E. and Rongo, C. (2004). The unfolded protein response regulates glutamate receptor export from the endoplasmic reticulum. *Mol. Biol. Cell* **15**, 4818-4828.

Sieburth, D., Madison, J. M. and Kaplan, J. M. (2007). PKC-1 regulates secretion of neuropeptides. *Nat. Neurosci.* **10**, 49-57.

Souid, S., Lepesant, J. A. and Yanicostas, C. (2007). The xbp-1 gene is essential for development in Drosophila. *Dev. Genes Evol.* **217**, 159-167.

Tanudji, M., Hevi, S. and Chuck, S. L. (2002). Improperly folded green fluorescent protein is secreted via a non-classical pathway. *J. Cell Sci.* **115**, 3849-3857.

Todd, D. J., Lee, A. H. and Glimcher, L. H. (2008). The endoplasmic reticulum stress response in immunity and autoimmunity. *Nat. Rev. Immunol.* **8**, 663-674.

Urano, F., Wang, X., Bertolotti, A., Zhang, Y., Chung, P., Harding, H. P. and Ron, D. (2000). Coupling of stress in the ER to activation of JNK protein kinases by transmembrane protein kinase IRE1. *Science* **287**, 664-666.

Urano, F., Calfon, M., Yoneda, T., Yun, C., Kiraly, M., Clark, S. G. and Ron, D. (2002). A survival pathway for Caenorhabditis elegans with a blocked unfolded protein response. *J. Cell Biol.* **158**, 639-646.

Vandenberghe, W. and Bredt, D. S. (2004). Early events in glutamate receptor trafficking. *Curr. Opin. Cell Biol.* **16**, 134-139.

Vidal, R. L., Figueroa, A., Court, F. A., Thielen, P., Molina, C., Wirth, C., Caballero, B., Kiffin, R., Segura-Aguilar, J., Cuervo, A. M. et al. (2012). Targeting the UPR transcription factor XBP1 protects against Huntington's disease through the regulation of FoxO1 and autophagy. *Hum. Mol. Genet.* **21**, 2245-2262.

Yamamoto, K., Sato, T., Matsui, T., Sato, M., Okada, T., Yoshida, H., Harada, A. and Mori, K. (2007). Transcriptional induction of mammalian ER quality control proteins is mediated by single or combined action of ATF6alpha and XBP1. *Dev. Cell* **13**, 365-376.

Ye, J., Rawson, R. B., Komuro, R., Chen, X., Davé, U. P., Prywes, R., Brown, M. S. and Goldstein, J. L. (2000). ER stress induces cleavage of membrane-bound ATF6 by the same proteases that process SREBPs. *Mol. Cell* **6**, 1355-1364.

Yoneda, T., Imaizumi, K., Oono, K., Yui, D., Gomi, F., Katayama, T. and Tohyama, M. (2001). Activation of caspase-12, an endoplastic reticulum (ER) resident caspase, through tumor necrosis factor receptor-associated factor 2-dependent mechanism in response to the ER stress. *J. Biol. Chem.* **276**, 13935-13940.

Yoshida, H. (2007). ER stress and diseases. *FEBS J.* **274**, 630-658.

Zhao, H., Cao, Y. and Grunz, H. (2003). Xenopus X-box binding protein 1, a leucine zipper transcription factor, is involved in the BMP signaling pathway. *Dev. Biol.* **257**, 278-291.

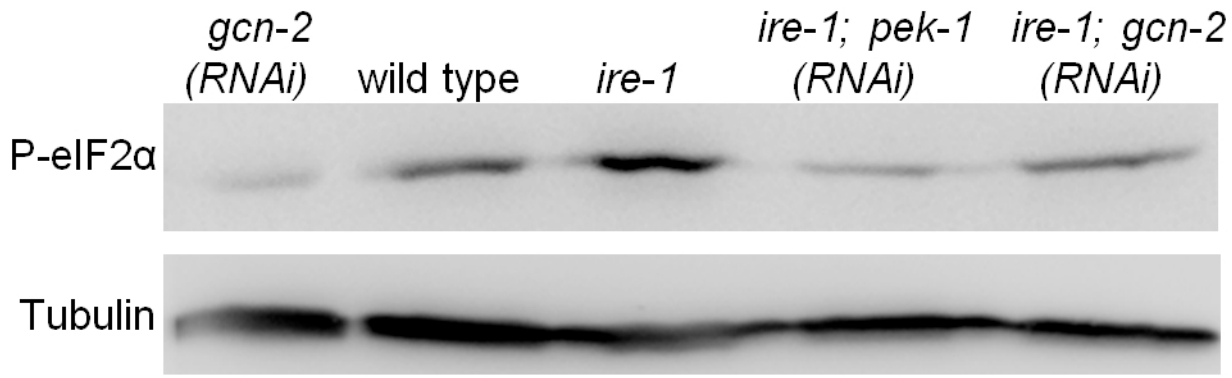

Fig. S1. Phosphorylation of eIF2α by PEK-1 is increased in *ire-1* mutants. Representative western blot of phosphorylated eIF2α and tubulin of day-0 wild-type animals and *ire-1* mutants treated with control, *pek-1* or *gcn-2* RNAi. Note that whereas in wild-type animals eIF2α phosphorylation was mostly *gcn-2* dependent, in *ire-1* mutants eIF2α phosphorylation was mostly *pek-1* dependent. This experiment was repeated three times with similar results.

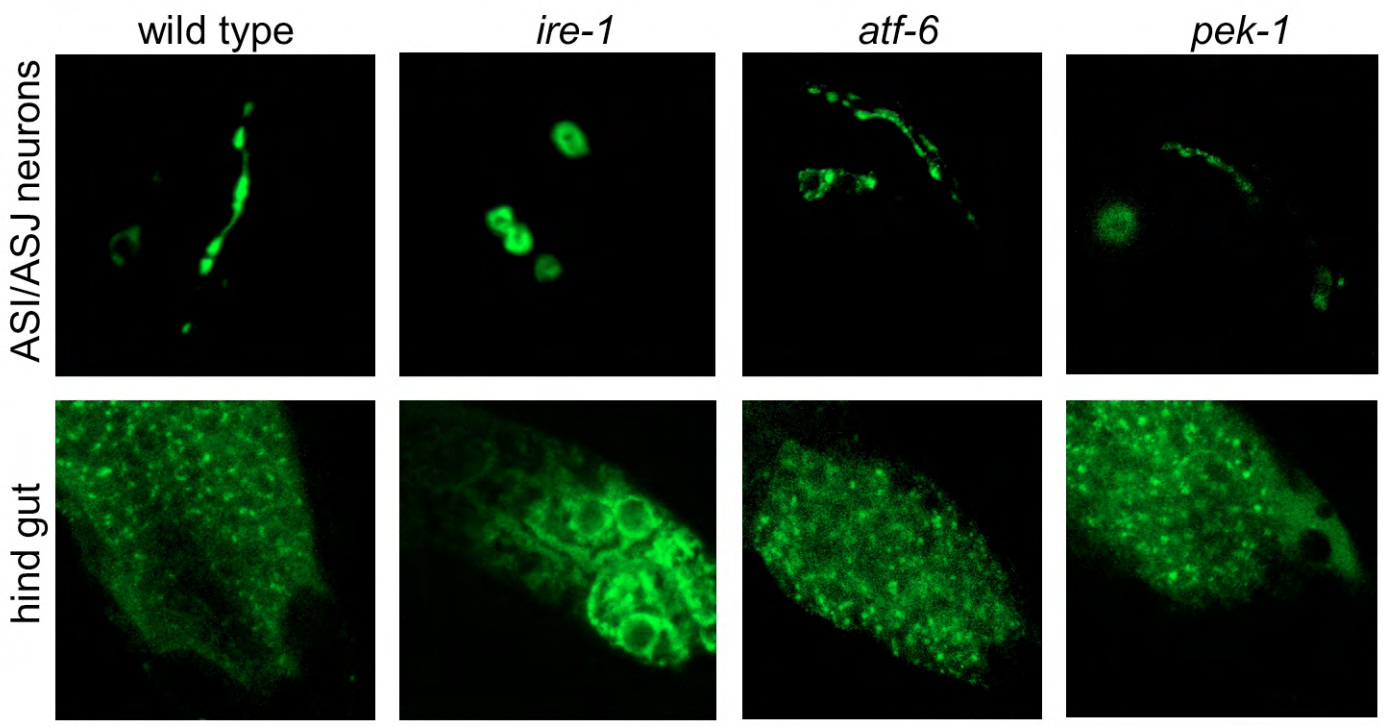

Fig. S2. *ire-1* deficiency alters DAF-28::GFP pattern within producing cells. Confocal fluorescence micrographs (630×) of ASI/ASJ neurons and hind gut in day-3 wild-type animals and in *ire-1, atf-6* and *pek-1* mutants.

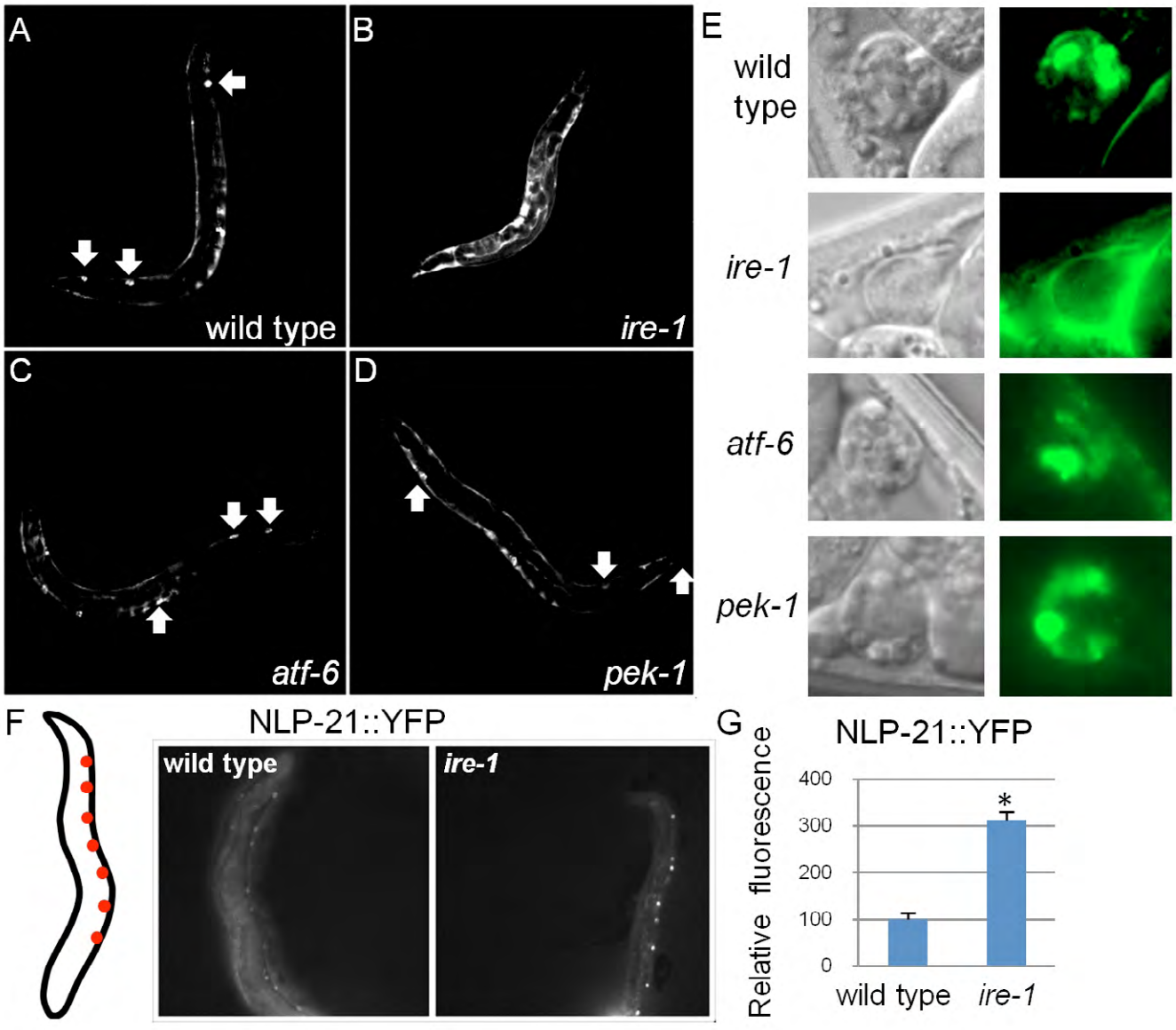

Fig. S3. *ire-1* deficiency alters *Pmyo-3*::ssGFP and *Punc-129*::NLP-21::YFP expression patterns. (A-D) Representative fluorescence micrographs (100×) of day-1 adults harboring an integrated *Pmyo-3*::ssGFP transgene in a wild-type, *ire-1(ok799), atf-6(ok551)* or *pek-1(ok275)* background. Wide arrows point to GFP-labeled coelomocytes. Note that in *ire-1* mutants no GFP-labeled coelomocytes were detected. Instead accumulation of GFP within the body cavity was detected. (E) Representative Nomarski and fluorescence micrographs (630×) of coelomocytes in day-1 adults harboring an integrated *Pmyo-3*::ssGFP transgene in the indicated genotypes. GFP was detected surrounding the coelomocytes rather than within the coelomocyte cells of *ire-1* mutants. (F) Representative fluorescence micrographs (100×) of day-1 adults expressing the *nlp-21::yfp* transgene using the ventral-cord *Punc-129* promoter. Scheme of predicted *unc-129* expressing cells (red) is shown to the left. (G) Bar graph of mean relative fluorescence in the ventral cord neurons of wild type and *ire-1* mutants. Fluorescence was measured in at least 20 animals per genotype. Similar results were obtained in three independent experiments. Asterisk marks Student's *t*-test value of $P<0.0001$.

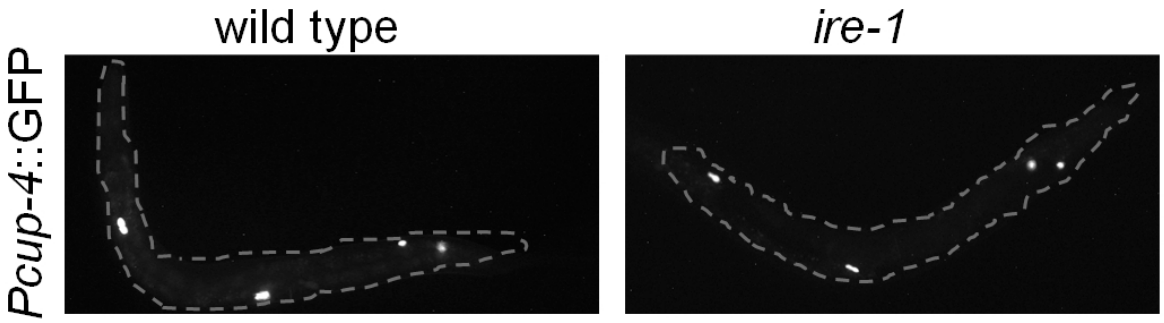

Fig. S4. Coelomocytes do exist in *ire-1* mutants. Representative fluorescence micrographs (100×) of day-1 adults harboring an integrated transgene expressing GFP under the coelomocyte-specific *cup-4* promoter.

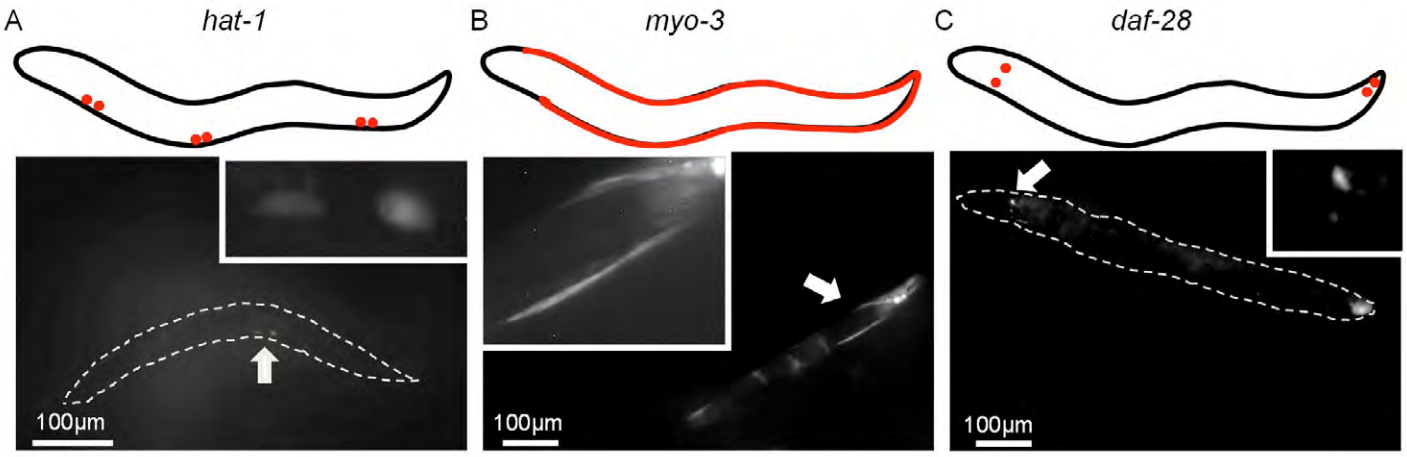

Fig. S5. Tissue-specific rescue of *ire-1* activity. Representative fluorescence micrographs of *Phsp-4::gfp* in *ire-1* mutants expressing *ire-1* under *hat-1*, *myo-3* and *daf-28* tissue-specific promoters. (A) Scheme and representative fluorescence micrograph (200×) of young animals expressing *ire-1* driven by the *hat-1* promoter. We note that *Phsp-4::gfp* induction was detected only in coelomocyte cells. No induction was detected outside of the coelomocytes in more than 50 animals examined. Induction was always detected only in 1-2 coelomocyte cells per animal. (B) Scheme and representative fluorescence micrograph (100×) of young animals expressing *ire-1* driven by the *myo-3* promoter. We note that *Phsp-4::gfp* induction was detected only in muscle cells. More than 50 animals were examined. (C) Scheme and fluorescence micrograph (100×) of young animals expressing *ire-1* driven by the *daf-28* promoter. In all animals examined, *Phsp-4*::GFP expression was detected in a few head neurons (most likely the ASI/ASJ neurons). In some animals, *Phsp-4*::GFP expression was also detected in the hind gut. Note that due to the long exposure times, some autofluorescence, clearly distinguishable from the GFP signal, was detected as well. Wide white arrows point at *Phsp-4::gfp*-expressing cells whose magnified images are presented in the corresponding insets.

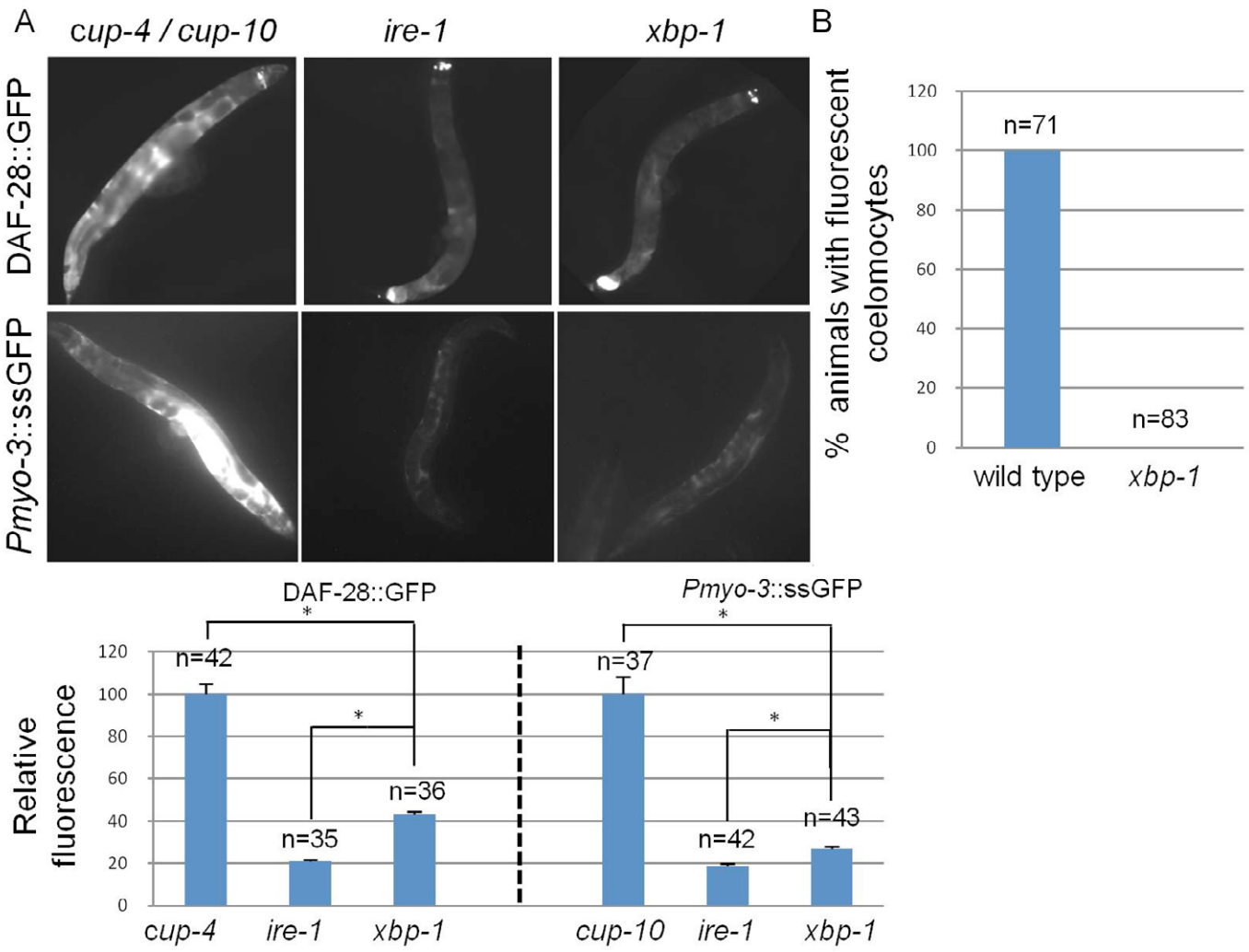

Fig. S6. *xbp-1* deficiency reduces accumulation of secreted proteins in the body cavity of coelomocyte-defective animals. (A) Representative fluorescence micrographs (100×) of day-3 adults harboring an integrated DAF-28::GFP transgene (upper panel), or day-1 adults harboring a *Pmyo-3*::ssGFP transgene (lower panel). Bar graphs of the mean whole body fluorescence in the corresponding strains is presented. Coelomocyte-defective *cup-4(ok837)* and *cup-10(ar479)* mutants accumulate fluorescent proteins in their body cavities. Coelomocyte-defective *ire-1(ok799*) and *xbp-1(tm2457)* mutants accumulate significantly less GFP in their body cavities. "n" indicates number of animals analyzed. Similar results were obtained in three independent experiments. Asterisks mark Student's *t*-test values of $P<0.0001$ of *xbp-1* mutants compared to wild-type animals and compared to *ire-1* mutants. (B) Percentage of wild-type animals and *xbp-1* mutants in which fluorescent coelomocytes were detected. "n" indicates number of animals analyzed.

Table S1. Worm strains

N_2

CF2473: *ire-1(ok799) II*;

CF3208: *xbp-1*(*tm2475*) *III*;

CF2921: *pek-1(ok275) X;*

CF2988: *atf-6(ok551) X*;

GR1455: *mgIs40[Pdaf-28::gfp];*

CF3222: *ire-1(ok799) II*; *mgIs40[Pdaf-28::gfp]*;

VB1605: *svIs69[Pdaf-28::DAF-28::GFP];*

SHK11: *ire-1(ok799) II*; *svIs69[Pdaf-28::daf-28::gfp] ;*

xbp-1(tm2457) III; svIs69[Pdaf-28::daf-28::gfp] ;

SHK38: *cup-4(ok837) III; svIs69[Pdaf-28::daf-28::gfp] ;*

SHK15: *ire-1(ok799) II*; *svIs69[Pdaf-28::daf-28::gfp] ;biuEx4[Pdaf-28::ire-1; pRF4(rol-6(su1006))];*

SHK17: *ire-1(ok799) II*; *svIs69[Pdaf-28::daf-28::gfp] ;biuEx3[Phat-1::ire-1; pRF4(rol-6(su1006))];*

SHK18: *ire-1(ok799) II*; *svIs69[Pdaf-28::daf-28::gfp] ;*

SHK47: *pek-1(ok275) X*; *svIs69[Pdaf-28::daf-28::gfp] ;*

SHK48: *atf-6(ok551) X*; *svIs69[Pdaf-28::daf-28::gfp] ;*

SHK49*: biuEx7[Pdaf-28::ssRFP::KDEL; pRF4(rol-6(su1006))];*

SHK50: *ire-1(ok799) II; biuEx7[Pdaf-28::ssRFP::KDEL; pRF4(rol-6(su1006))];*

GS1912:arIs37[Pmyo-3::ssGFP] I; dpy-20(e1282) IV; mtm-9(ar479) V;

SHK12: *arIs37[Pmyo-3::ssGFP] I; ire-1(ok799) II*;

arIs37[Pmyo-3::ssGFP] I; xbp-1(tm2457) III;

GS2495: *arIs37[Pmyo-3::ssGFP] I; cup-10*(ar479) *V*;

SHK13: *arIs37[Pmyo-3::ssGFP] I*; *ire-1(ok799) II*; *biuEx3[Phat-1::ire-1; pRF4(rol-6(su1006)] ;*

SHK14: *arIs37[Pmyo-3::ssGFP] I*; *ire-1(ok799) II*; *biuEx5[Pmyo-3::ire-1; pRF4(rol-6(su1006))] ;*

KP3947*: nuIs183[Punc-129::nlp-21::Venus; Pmyo-2::GFP] III;*

SHK21: *ire-1(ok799*) II; *nuIs183[Punc-129::nlp-21::Venus; Pmyo-2::GFP] III ;*

CL4176: *smg-1(cc546) I*; *dvIs27[pAF29(Pmyo-3/A-Beta 1-42/let UTR) + pRF4(rol-6(su1006))];*

SHK39: *smg-1(cc546) I*; *xbp-1(tm2457) III*; *dvIs27[pAF29(Pmyo-3/A-Beta 1-42/let UTR) + pRF4(rol-6(su1006))];*

SHK51: *smg-1(cc546) I*; *ire-1(ok799) II*; *dvIs27[pAF29(Pmyo-3/A-Beta 1-42/let UTR) + pRF4(rol-6(su1006))];*

SHK34: *arIs37[Pmyo-3::ssGFP] I; pek-1 (ok275) X*;

SHK33: *arIs37[Pmyo-3::ssGFP] I; atf-6 (ok5551) X;*

SHK29: *ire-1(ok799) II*; *cdIS42[Pcup-4::GFP; unc-119+];*

NP748: *unc119(ed3) III; cdIS42[Pcup-4::GFP; unc-119+];*

ire-1(ok799) II; *zcIs4[hsp-4::GFP]* V; *biuEx3[Phat-1::ire-1; pRF4(rol-6(su1006))];*

ire-1(ok799) II; *zcIs4[hsp-4::GFP]* V;*biuEx5[Pmyo-3::ire-1; pRF4(rol-6(su1006))] ;*

ire-1(ok799) II; *zcIs4[hsp-4::GFP]* V;*biuEx4[Pdaf-28::ire-1; pRF4(rol-6(su1006))] ;*

ire-1(ok799) is a null mutation in which three exons containing the kinase and endonuclease domains are deleted.

xbp-1(zc12) is a putative null mutation, a nonsense mutation that changes Q34 to an ochre stop, terminating it before its functional domains. Similarly to *xbp-1(tm2475)* null mutants, animals carrying zc12 are sensitive to ER stress and unable to induce transcription through the *hsp-4* promoter in response to ER stress.

atf-6(ok551) is a putative null mutation deleting 1,900 bp of genomic sequence, resulting in a protein missing the leucine zipper portion of the bZIP domain, the transmembrane domain, and the ER luminal domain.

pek-1(ok275) is a putative null mutation in which more than five exons are missing, resulting in the loss of a critical transmembrane domain.